Development and experimental testing of an integrated prototype based on Stirling, ORC and a latent thermal energy storage system for waste heat recovery in naval application

F. Catapano [a,*], A. Frazzica [b], A. Freni [c], M. Manzan [d], D. Micheli [d], V. Palomba [b], P. Sementa [a], B. M. Vaglieco [a]

[a] CNR - Institute of Science and Technology for Sustainable Energy and Mobility (STEMS), Napoli, Italy
[b] CNR - Institute of Advanced Energy Technologies "Nicola Giordano" (ITAE), Messina, Italy
[c] CNR - Institute of Chemistry of Organo Metallic Compounds (ICCOM), Pisa, Italy
[d] University of Trieste, Dept. of Engineering and Architecture, Trieste, Italy

HIGHLIGHTS

- Optimization of an integrated waste-heat recovery systems for naval uses.
- Integration of Stirling, ORC systems and a thermal storage system during a cruise.
- WHR control strategy satisfied the entire hot water demand through the heat storage.
- ORC and Stirling converted into electricity more than 10% of total energy recovered.

ARTICLE INFO

Keywords:
Ship energy system
WHR
ORC
Stirling engine
Latent heat thermal storage
Lab-scale prototype

ABSTRACT

This paper focuses on an advanced energy system, able to increase the overall efficiency of ships by recovering the heat wasted by the propulsion system. A small-scale prototype has been realized, developed, and tested under realistic operating conditions of boat during a winter and summer cruise. The main novelty of the research that has been presented in this paper lies in a significant contribution by developing an integrated dynamic device for electrical production and thermal energy storage. It is based on a 1000 cm^3 light duty compression ignition engine coupled with a properly adapted Stirling Engine (SE), an Organic Rankine Cycle group (ORC) and a latent Thermal Energy Storage system (TES). All the components have been managed by means of a specifically developed electronic control, simulating two standard cruise profiles. Scaled engine power data have been imposed to simulate port, manoeuvring and open sea navigation phases. The consumption of hot water has been obtained by considering the typical hourly use profile of a cruise ship.

It has been demonstrated that the proposed integrated system allows recovering all the thermal energy needed to satisfy the hot water request during the cruise, avoiding the use of auxiliary boilers. The results indicate a favourable effect because the recovered thermal energy represents the 7.7 % of the total energy consumed by fuel. The net electrical energy generated by ORC and Stirling engine resulted to be about 1 % of the total fuel energy consumption, respectively 0.8 % and 0.2 %. The developed prototype can be a useful tool in viability analysis and can easily be reproduced for several uses. In conclusion, the integration of different systems with an optimal integration and sizing of the thermal energy storage considerably improve the thermodynamic, economic and environmental results for future clean ships.

1. Introduction

The reduction of energy consumption in the field of maritime transport is an urgent need, due to the large use of fossil fuels and the related polluting emissions, which amount to up of 3 % of global CO_2 [1]. For this purpose, the regulations issued by the International Maritime Organization (IMO) provide for the fulfilment of parameters such

* Corresponding author.
E-mail address: francesco.catapano@stems.cnr.it (F. Catapano).

Accepted 4 February 2022

Nomenclature

1D	mono-dimensional
3D	three-dimensional
CFD	Computational Fluid Dynamics
CHP	Combined Heat and Power
CI	Compression Ignition
Conf-i	ith configuration of the heat exchanger
CR	Common Rail
Cyl	Cylinder
E	Energy [J]
ECU	Electronic Control Unit
eff	effective
GWP	Global Warming Potential
HE	Heat exchanger
HTFW	High-Temperature Fresh Water
HTLW	Low-Temperature Fresh Water
ICE	Internal Combustion Engine
IMO	International Maritime Organization
$\dot{m}$	mass flow rate [kg/s]
m	mass [kg]
ODP	Ozone Depletion Potential
ORC	Organic Rankine Cycle
PCM	Phase-change Material
$\dot{Q}$	heat rate [kW]
Q	heat [J]
Q_{cw}	heat from cooling water
Q_{eg}	heat from exhaust gas
Q_{loss}	heat losses
SE	Stirling Engine
SEEMP	Ship Energy Efficiency Management Plan
T	Temperature [K]
T HE	temperature at the center of the heat exchanger
T_IN HE	temperature of exhaust gas at the inlet of the heat exchanger
T_OUT HE	temperature of exhaust gas at the outlet of the heat exchanger
T_Users	temperature of the domestic hot water
TES	Thermal Energy Storage
$T_{IN,cool}$	temperature at the inlet of the SE cooling system
$T_{OUT,cool}$	temperature at the outlet of the SE cooling system
t_{source}	hot water temperature entering the ORC
Tstorage	temperature in the center of the Thermal storage
Tstorage_DN	temperature in the lower position of the Thermal storage
Tstorage_UP	temperature in the upper position of the Thermal storage
v	velocity [m/s]
V	volume [m^3]
W	work [J]
WHR	Waste Heat Recovery
η	efficiency [%]
η_{th}	thermal efficiency [%]

as the Energy Efficiency Design Index (EEDI) for new ships and the Ship Energy Efficiency Management Plan (SEEMP) for all ships [2,3].

Accordingly, several measures for increasing the sustainability of maritime field by 2050 have been put in effort, which include not only the use of alternative fuels (ammonia, hydrogen, electricity) but also a wider set of options for energy efficiency from traditional systems on board [4,5]. A comprehensive study on the different technologies and measures for the reduction of greenhouse gases (GHG) emissions in vessels is presented in [6]. The possible alternatives are rated in terms of cost and potential for savings. Among the available options, the most attractive ones in terms of the amount of GHG emissions avoidable are those related to propulsion and to energy sources utilization. Better use of energy sources on board includes Waste Heat Recovery (WHR) from multiple sources (main and auxiliary engines, generators, boilers…). Several reviews are available in the literature on the topic [7,8]. Indeed, in a typical marine Diesel engine, more than 50 % of the fuel energy is lost through the exhaust gas, at medium temperature level (250–300 °C), and the cooling and lubrication circuits, at low temperature level (60–90 °C) [9]. WHR allows increasing the overall energy efficiency by partly converting the heat dumped to the environment by the primary cycle in both thermal and electric useful energy. Greater efficiency, obtained optimally exploiting the multiple available energy sources, translates into fuel savings and lower polluting emissions. Several technologies are attractive for WHR application on board. The widest applied ones are traditional steam turbines operated in conventional Rankine cycles. While the economic profitability of Rankine cycles and their application on board for Internal Combustion Engines (ICEs) was widely analysed in the literature, [9-11], still some critical issues have to be faced in the maritime sector. They are mainly due to the temperature level on board which not always allows efficient operation of the power cycle [8] and the need to comply with fluorinated gases (F-gas) regulations [10]. Additionally suggested technologies include fuel cells [12], for which, however, technical challenges and policy/standardisation barriers are even higher. In addition, Brayton cycles and supercritical CO_2 Brayton cycles have been studied [13,14], but among the difficulties reported for the specific application in the maritime sector, there is the need to adapt to continuously changing temperature and power levels.

As can be derived from the above reported literature analysis, the main features making attractive a system able to increase the energy efficiency on board through waste heat are [6]: possibility of retrofitting in existing vessels with low-cost measures (i.e. without major modifications on the propulsion system), utilization of waste heat at different temperature levels, possibility of using buffers to compensate for power fluctuation in the heat sources and use, in closed cycle systems, of low Global Warming Potential (GWP) and Ozone Depletion Potential (ODP) working fluids.

Within the field of power cycles, then, a possible alternative is the use of Organic Rankine Cycle (ORC) systems. These units allow recovering heat at lower temperatures, compared to standard Rankine cycles, due to the thermodynamic properties of a properly chosen organic working fluid [15,16]. In particular, various studies confirm that the use of ORCs driven by the wasted thermal energy of ship Diesel engines is a very attractive technology for an effective fuel saving [17-19]. In such a way, a noticeable reduction of CO_2 emissions is obtained per kWh of produced energy, as shown in [20]. Utilization of multi-stage ORC systems, able to recover energy from exhaust flows at different temperatures, can further increase their efficiency [21]. It is worth noticing that, for ORC, several operating fluid options that comply with low-GWP and low-ODP constraints are currently being studied and begin to be available, also as drop-in replacements [22-24]. Another option that has not been widely explored so far is represented by the Stirling Engines (SE), in which work is generated by the cyclic expansion and compression of working gases as air, helium, nitrogen or hydrogen between a hot and a cold source named heater and cooler, respectively. The variation of the working gas pressure is converted into mechanical work via a connecting rod and crankshaft system, which connects two working pistons or a displacer and a working piston [25], according to the engine configuration. The main barrier to the use of SE so far is probably due to the low thermal level of the waste heat from marine Diesel engines. Anyway, as

suggested in [26,27] the adoption of SE directly powered by the exhaust gases of the main engine can be considered an efficient way to further improve the system efficiency. In fact, SE could be a promising solution for WHR from ICE because of its compact design, easy maintenance, handling and safety as well as its operating flexibility over a wide temperature range and good efficiency. Several applications in solar-powered cycles have been proposed so far [28-30] but the application in maritime environment with good efficiency is also feasible, as experimentally proven by some of the authors in [31].

As stated above, one of the other challenges that need to be overcome in order for such systems (ORC, SE) to properly work on board is the need to compensate for power and temperature fluctuations of the WHR systems. Therefore, there is a strong need for the development of advanced Thermal Energy Storage (TES) solutions, in order to respond to peak demand and to improve the system management [32,33]. So far, the applications of TES in the naval sector are still limited for two main reasons, namely, the huge volume required to store enough energy and the abundant waste heat available on-board, which usually overcomes the heating demand, thus reducing the need of storing it. Nevertheless, when the ships are docked in port, auxiliary boilers can be needed to cover the continuous heating demand, if the heat recovery from the gensets is not sufficient, penalizing the energy efficiency of the ship. Accordingly, storing part of the excess heat during the cruise phases, to employ it during the port phases can reduce the fuel consumption due to the auxiliary boilers, as shown as an example in [34] for ground applications. Baldi et al. [35], presented a preliminary study aiming at a techno-economic analysis of the integration of a high temperature TES on board of a merchant vessel. In this case, the required temperature for the on-board needs is well above 100 °C, having to heat up the fuel tanks besides providing the space heating. For this reason, authors considered a large tank using thermal oil as sensible TES medium. The performed calculations, based on available consumption data of a real vessel, demonstrated the possibility of reducing the fuel consumption when the vessel is docked in the port from 60 % to 90 %, if the storage tank size varies from 500 m^3 to 2500 m^3. Fang et al. [36] investigated the operation of a hybrid electrical/thermal storage to be integrated in a cruise ship, analysing an innovative management strategy, based on two-stage operation. This approach considers that the time-scale of the electric and thermal demand are different, accordingly the electric generation/storage was managed on hourly basis, while the thermal generation/storage was based on 20 min time-scale. The comparison against a single-stage operation approach, under real conditions, demonstrated the relevant role of the hybrid storage in enabling both economic and environmental improvements in cruise ships characterized by comparable share of thermal and electric energy demand. In this context, in order to further increase the attractiveness of TES on board, the employment of latent or hybrid sensible/latent storage systems, can be considered as a suitable solution to achieve high heat storage power density, allowing meeting the naval space requirements [37].

From what reported so far, it is clear that the most efficient way for energy recovery in the maritime transport is through a combined system, that should include a thermal storage and multiple power cycles. So far, in the literature, only few examples of such systems have been reported and mainly theoretical applications have been found with reference to marine engines. As an example, Gnes et al. [36] have defined a multi-objective procedure for the integrated optimization of ORC/SE energy recovery system on board of a large cruise ship, using 50 kW SE groups. They found that the optimal number of groups for effectively reducing the fuel consumption and emissions during the cruise is 18–20. A combination of a latent TES with an ORC is presented in [38], but it is based on simulations with the aim of optimising the working fluid of the ORC. An inverted Brayton cycle (IBC) for waste heat recovery from ICE is presented in [39] in which the IBC is used as topping cycle from the turbocharger but the foreseen application is only in temperate weather. A combined system with ORC, steam Rankine cycle and power turbine is discussed in [40]. The most notable result of the paper is that, despite the complication of the system, the possibility of using waste heat from different sources allow a low payback time (<7 years). At the same time, the main limitation of the proposed system is that it requires high load of the engine for efficient operation. A multi-objective design for increasing the WHR efficiency in cruise ship is carried out in [41] and it was found out that maximization of heat recovery only occurs though proper allocation of load and switching from the use of standard boilers and standard heating/cooling systems to more complex but yet thermally driven ones.

Starting from the literature review presented above, a clear gap was then identified: multi-systematic approaches for WHR are missing or not extensively discussed and, most importantly, mainly theoretical studies and numerical models are available. For this reason, the present paper reports the design and experimental testing of an advanced energy system able to increase the overall efficiency of ships by recovering waste heat from the propulsion engine. Experimental tests have been carried out on a laboratory-scale testing facility designed and assembled at CNR-STEMS. Firstly, the testing facility and all its main sub-systems (IC engine, ORC, SE and TES) are introduced. Afterwards, we describe the advanced control tool developed in order to manage and optimize the energy flows as a function of the user demand. The system has been previously tuned by finding the best values of the free adjustment parameters of all the components. Finally, experiments have been carried out simulating two typical one-week cruises. The engine load and the hot water request were adjusted, on a reduced time scale, according to realistic operating data of a cruise vessel.

2. System description

The schematic of the innovative system for the WHR from the ship propulsion engine is presented in Fig. 1. Overall design of the system was carried out considering the integrated energy production and recovery processes on a cruise vessel. One peculiarity of cruise ships is the balance between the energy used for propulsion and those used for other services, with about 46 % of the total energy used for propulsion, 27 % for heat and 27 % for electric power generation [42]. Accordingly, the provision out of the waste heat system of vapour, hot water for hotel users and electricity was considered. The exhaust gases from the Diesel/gas engine are firstly used to drive the SE, which produces electricity. The outlet gases from the SE flow in a steam economizer that, in turn, drives the ORC, allowing further electricity production. The TES can be charged directly from the coolant circuit of the Diesel engine or from the heat rejected by the ORC. According to the specific design of the steam economizer and TES, heat for the various users on board can be

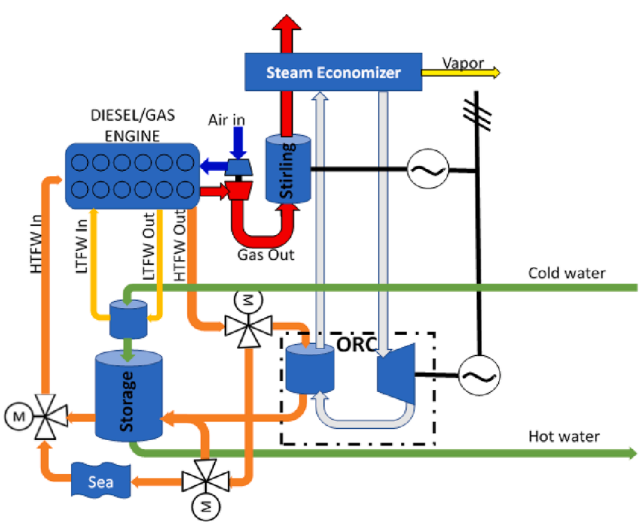

Fig. 1. Schematic of the waste heat recovery system.

recovered and stored at different temperature levels.

Based on the overall system presented in Fig. 1, a lab-scale prototype of the energy recovery system was realized at CNR-STEMS, described in Fig. 2. A 1000 cm^3 3-cylinder Diesel engine was chosen as a substitute of the propulsion engine of the ship. Other core components are a TES prototype with embedded Phase-Change Materials (PCMs), a commercial ORC and a commercial SE, both properly adapted for the specific application. The exhaust line of the Diesel engine was equipped with a properly designed gas-to-gas heat exchanger in order to provide thermal energy to the SE. In particular, it was designed maintaining the exhaust pipe internal section, so as not to modify the back pressure to the engine. Moreover, the cooling system of the Diesel engine was modified including a three-way valve used to send the hot water from the engine either to the ORC or to the TES, in order to maximize the heat recovery. The hot water to the ORC passes also through a gas-to-water heat exchanger at the exhaust of the SE, in order to simulate the steam economizer of the ship. This increases the water temperature to the ORC enhancing the efficiency of the system.

3. System components

The first part of the research activities was devoted to the development and characterization of the core components of the innovative WHR system, which are described in the following sections.

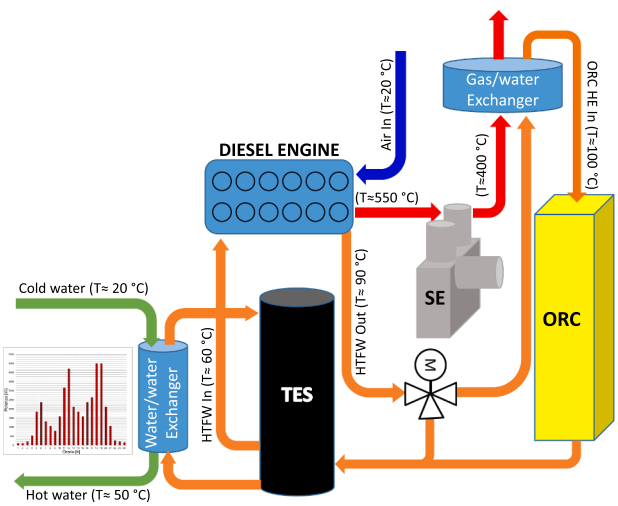

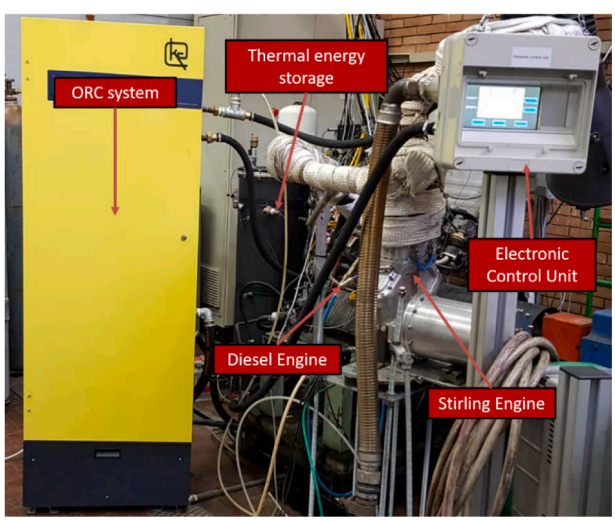

Fig. 2. Prototype layout and practical realization.

3.1. The internal combustion engine

The three-cylinder compression ignition engine used for the prototype is a naturally aspirated unit, fueled with an electronically controlled common rail direct injection system. All the operations are managed by a closed Electronic Control Unit (ECU). Table 1 reports the main technical details of the ICE. The engine has been fed with commercial Diesel fuel, but it could operate also with biodiesel and in dual fuel mode [43]. It is capable of developing a power of about 16 kW at 3400 rpm. Air flow rate and fuel consumption can be continuously measured in order to estimate the exhaust gas mass flow rate.

Fig. 3 shows the thermal balance achieved on the engine at different rotation speeds, at full and medium load. More detail in [43]. The fraction of combustion thermal power converted into useful power (P) and the fraction released into the environment through different thermal flows depends on the operating point of the engine.

At full load, P varies between 32 % at 3600 rpm and 35 % at 2600 rpm. At medium load, the power varies between 25 % at 3200 rpm and 32 % at 2000 rpm. The percentage of heat output that could be recovered from the cooling water (Q_{cw}) decreases as the load increases. Furthermore, at full load, Q_{cw} decreases with increasing rotation speed and varies between 19 % at 1600 rpm and 13 % at 3600 rpm. At medium load, Q_{cw} shows a less defined trend with rotation speed with a maximum of 30 % at 2000 rpm and a minimum of 18 % at 1600 rpm. As regards the fraction of thermal power recoverable from the exhaust gases (Q_{eg}), higher values are observed at full load. Furthermore, for both loads, Q_{eg} has an increasing trend with the rotation speed: at full load it varies between 12 % at 1600 rpm and 18 % at 3600 rpm while at medium load Q_{eg} varies between 5 % and 13 % at 1600 and 3600 rpm respectively. At all operating conditions, a significant amount of heat is permanently lost.

3.2. The Stirling engine

A commercial SE has been installed at the exhaust of the ICE in the lab-scaled prototype of the WHR system. It is a two-cylinder gamma-type unit, made of aluminum, having both the power piston and the displacer mounted on the same crankshaft, with a phase angle of 88 °, a schematic of one cylinder of the SE is reported in Fig. 4. The expansion and the compression spaces are joined by means of a connecting pipe. The heater consists of two tubular sets, each composed of 21 steel tubes with three different lengths. The regenerator is filled with a copper foam of high volumetric porosity, equal to 96.5 %. The cooler is a finned water-jacketed heat exchanger. The working gas is helium (He). The main SE specifications are summarized in Table 2.

The original SE has been partially modified in order to improve its efficiency in the temperature range of 500 °C – 400 °C available at the ICE exhaust, lower than its design range of 700 °C – 800 °C. Particularly, the heater was completely re-designed by means of a synergic experimental and numerical approach.

A proper thermally insulate cap was designed to realize a shell-and-tube heat exchanger. Three configurations, indicated as Conf-1, Conf-2 and Conf-3 and shown in Fig. 5 (a), (b), (c), have been designed and tested. Conf-1 is characterized by one inlet and one outlet on the

Table 1
Internal combustion engine specifications.

Engine type	Compression ignition
Number of cylinders	3, in-line
Bore [mm]	75
Stroke [mm]	77.6
Displacement [cm^3]	1028
Compression ratio [-]	17.5:1
Injection system	Direct, Common Rail
Max. injection pressure [bar]	1400
Intake	Naturally aspirated

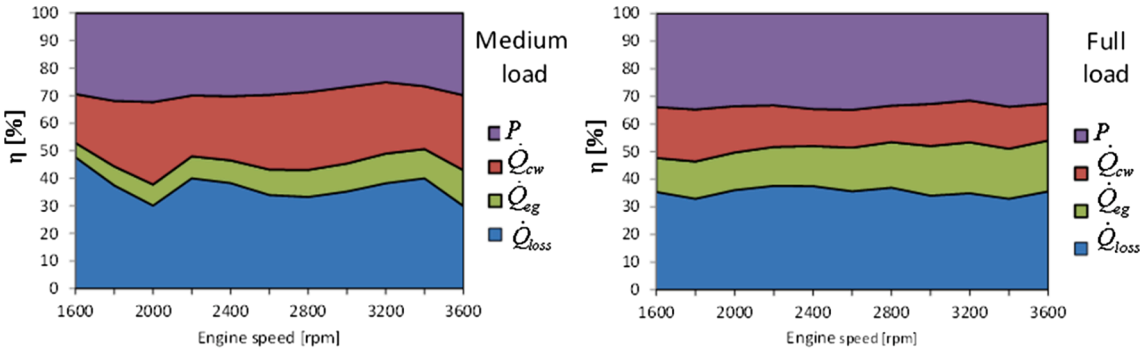

Fig. 3. Thermal balance of the Diesel ICE at different speeds at medium and maximum load.

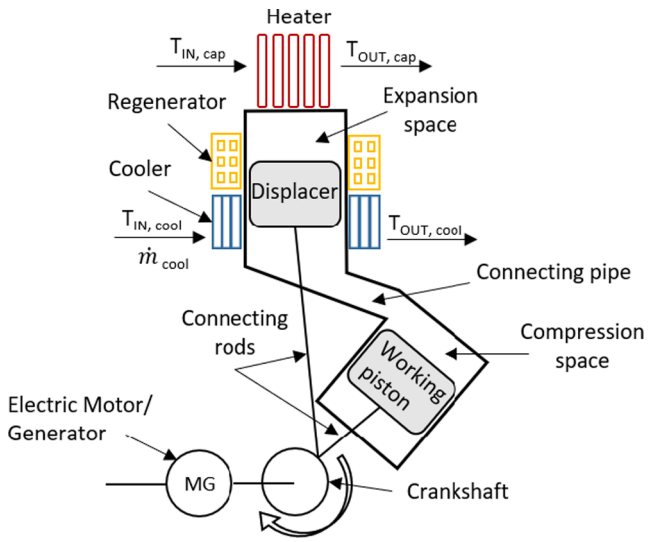

Fig. 4. Schematic of a single cylinder of the gamma type SE used in this study.

Table 2
Main features of the SE used in this study.

Engine type	Gamma Stirling
Number of working cylinders	2
Working piston bore [mm]	75
Working piston stroke [mm]	35
Displacer bore [mm]	75
Displacer stroke [mm]	50
Phase angle [deg]	88
Working gas	Helium
Coolant	Water

smallest surfaces of the cap. Conf-2 has one inlet on the lower part of the middle face of the cap, between the two tube bundles of the cylinder, and two outlets on the lateral surfaces, while Conf-3 has the same inlet section of Conf-2 but only one central upward outlet. Conf-2 and Conf-3 are symmetrical with respect to the cylinders while in Conf-1 the exhaust gas flows first on the tube bundles of one cylinder and then hits those of the second one. Moreover, Conf-2 and Conf-3 have an inlet section with a truncated cone shape while Conf-1 has a circular section.

The SE was equipped with thermocouples to measure the exhaust gas temperatures at the inlet and the outlet, as well as inside the cap. A pressure sensor allowed to set the working gas charge pressure. A flow meter and two thermocouples controlled the flow rate and both the inlet and outlet temperatures of the cooling water. An electric generator was coupled to the SE crankshaft. More details about sensors used are reported in section 3 in Table 6.

Table 3 summarizes the experimental conditions and the performance data measured for the three configurations of the heater. Mean pressure of the working fluid was fixed at 7.0 bar and the cooling water flow rate at about 450 kg/h. ICE was set to full load at 3400 rpm, corresponding to 16 kW of brake power, which is the condition selected for simulating the ship cruise condition.

In these conditions, the cap inlet temperature, $T_{IN, cap}$, has been very close in each test at about 830 K, while the cap outlet temperature, $T_{OUT, cap}$, in Conf-1 was higher of about 20 K than in both Conf-2 and Conf-3. The total produced mechanical power, $\dot{W}_{mec}$, resulted the highest for Conf-2, 0.350 kW, due to a better fluid-dynamic coupling between

Table 4
Main 3D model results in terms of temperature and heat transfer in the SE heater.

Heat Exchanger	$T_{He, OUT}$ [K]		$\dot{Q}_{He,IN}$ [kW]		$\dot{Q}_{He,IN}$ [kW]
	CYL 1	CYL 2	CYL 1	CYL 2	Tot
Conf-1	564	494	1.25	0.64	1.89
Conf-2	511	511	1.15	1.15	2.30
Conf-3	514	514	0.89	0.89	1.78

Table 5
Technical data of the selected Kaymacor ORC group.

Model	4 kW
Net electrical power [kW]	4
Input thermal power [kW]@ 170 °C	37
Output thermal power [kW]@ 50 °C	30
Voltage [V] @ 50 Hz	230
Hot fluid input temperature [°C]	80–170
Hot fluid nominal flow [kg/s]	0.26
Cold water output temperature [°C]	20–90
Cold water nominal flow [kg/s]	0.35
Size [cm]	45 × 60 × 172

Table 3
Experimental results with different configurations of the SE heater.

Heat exchanger	P_{He} [bar]	$T_{IN, cap}$ [K]	T_{cap} [K]	$T_{OUT, cap}$ [K]	$\dot{m}_{cool}$ [kg/h]	$T_{IN, cool}$ [K]	$T_{OUT, cool}$ [K]	$\dot{W}_{mec}$ [kW]	η_{tot} [%]
Conf-1	7.0	832.4	715.8	698.3	444	288.5	294.8	0.275	6.5
Conf-2	7.0	827.8	708.5	680.8	450	288.1	294.6	0.350	6.8
Conf-3	7.0	828.3	711.7	681.7	450	288.3	294.5	0.275	5.4

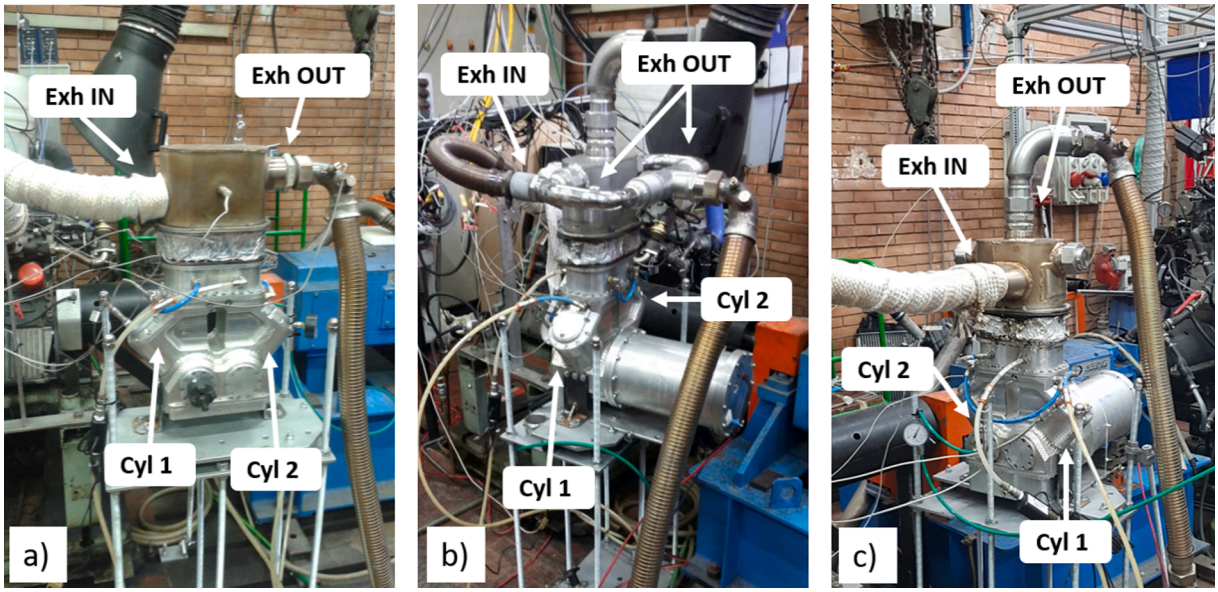

Fig. 5. View of the tested configurations of the SE gas–gas heat exchanger: Conf-1 (a), Conf-2 (b) and Conf-3 (c).

Table 6
Main features of the sensors and instruments of the monitoring and control system.

Quantity	*Sensor/Instrument*	*Range*	*Accuracy*
Exhaust gas temperature	K-type thermocouples	–270 ÷ 1260 [C°]	± 1.1 °C or 0.4 %
SE cooling water flow	Ultrasonic	0–25 [l/min]	3 % of reading
SE generator voltage	Resistive divider	0 – 50 [V]	1 % of reading
SE generator current	Hall current transducer	0 – 50 [A]	0.65 % of reading
Stirling Pressure	Piezoresistive absolute	0 – 10 [bar]	± 0,5 % FS max
TES water flow	Magnetic induction	0–40 [l/min]	± 2 % of FS
TES water temperature	T-type thermocouples	−184 ÷ 370 [C°]	± 1.1 °C or 0.4 %
ORC working fluid temperatures	Kongsberg Pt1000	–200 ÷ 600 [C°]	Class A
ORC working fluid evap. pressure	EWPA transducer	0 – 30 [bar]	± 0,25 % FS max
ORC working fluid cond. pressure	EWPA transducer	0.5 – 7 [bar]	± 0,25 % FS max

engine exhaust and SE operating fluid. Table 3 reports also the global SE efficiency (η_{tot}) evaluated as:

$$\eta_{tot} = \frac{\dot{W}_{mec}}{\dot{Q}_{exh}} \cdot 100 \tag{1}$$

and

$$\dot{Q}_{exh} = \frac{\dot{m}_{exh}}{3600} \cdot c_{p,exh} \cdot \left(T_{IN,cap} - T_{OUT,cap}\right)_{\mathrm{SE_{on}}} \tag{2}$$

where $c_{p,exh}$ is the specific heat at constant pressure for the ICE exhaust gas at T_{cap} and $\dot{m}_{exh}$ is the mass flow rate. Many other details about the experimental conditions and results have been published in [31]. The best configuration of the HE was the Conf-2 both in terms of produced power and efficiency and it has been used in the final WHR system configuration.

On the other side, experimental results give no information about the actual heat distribution inside the heat exchanger; therefore, a hybrid one-three dimensional (1D-3D) numerical approach was used in order to deepen the comprehension of the heat transfer in the cap-heater system. A 3D numerical model in COMSOL Multiphysics® was developed, and the balance equations of heat transfer and fluid flow interfaces have been solved in the hypothesis of non-isothermal flow. The experimental results were considered as boundary condition for the exhaust flow in the cap, particularly temperature and gas velocity at the inlet and pressure at the outlet. For the He in the heater, pressure and velocity values have been predicted using the well-established 1D Urieli adiabatic model [44]. Even if more complex models are reported in literature [45-47], the simpler ideal adiabatic analysis, adjusted according to the actual geometry, has been deemed sufficient for this study.

3D numerical results in term of velocity streamlines and temperature fields expressed in Kelvin are shown in Fig. 6 for Conf-1 and Conf-2 of the HE, respectively on the left and on the right. It is possible to note a completely different temperature distribution inside the tubes bundle of Conf-1 with respect to Conf-2, for which only half of the domain is depicted as it is symmetric with respect to the yz plane.

The temperature distribution of He in Conf-1 is extremely asymmetric. This is because the exhaust gas flows through the first cylinder (Cyl1) before entering the second one (Cyl2). He in Cyl1 gets 1.25 kW, about double the thermal power exchanged in Cyl2, as reported in Table 4. Temperature distribution Conf-3 is not shown in Fig. 6 as quite similar to Conf-2. Both are symmetrical with respect the cylinders but, Conf-2 allow the He to subtract about 23 % more heat in comparison with Conf-3 and 18 % than Conf-1. These numerical results are in good agreement with the measured mechanical power reported in Table 3, where the $\dot{W}_{mec}$ for Conf-2 is about 21 % higher than that of Conf-1 and Conf-3.

This analysis confirmed the Conf-2 as the best configuration of the SE heat exchanger. Moreover, it validated the capability of this simplified numerical methodology to model different geometries of the ICE-SE coupling system with reduced computational time and costs. It could allow further improving the heat recovery from ICE to SE also considering various engine regimes, sizes or models. The complete study about the SE heat exchanger modelling and optimization has been published in [31].

3.3. The thermal energy storage sub-system

A lab-scale (i.e. 100 dm^3) hybrid sensible/latent TES was integrated in the system. As shown in Fig. 7 it is based on a cylindrical vertical tank embedding up to 20 macro-capsules filled with the commercial PCM S58, a hydrated salt with nominal melting temperature of 58 °C and latent heat of 140 kJ/kg, provided by the company PCM Products. The

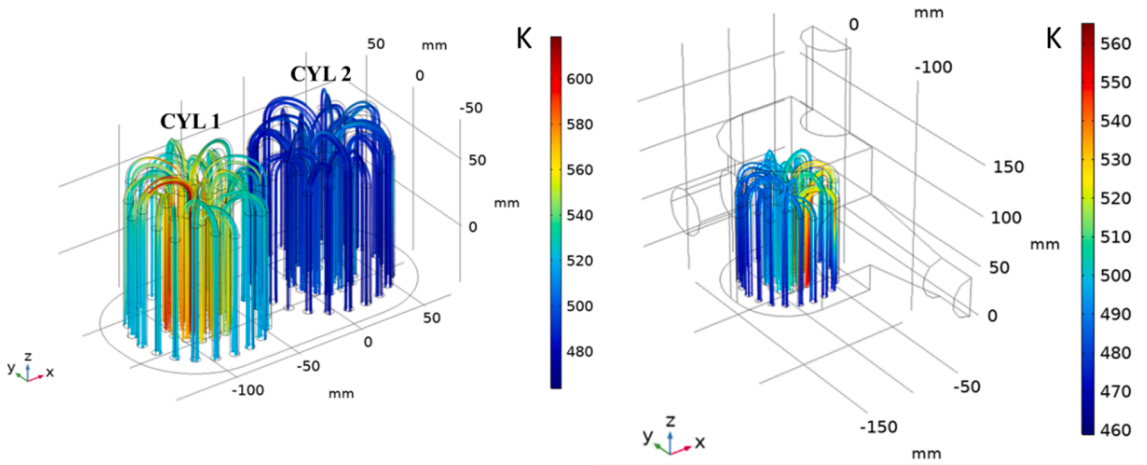

Fig. 6. Velocity streamlines and temperature fields in K in the heater for Conf-1 (left) and Conf-2 (right).

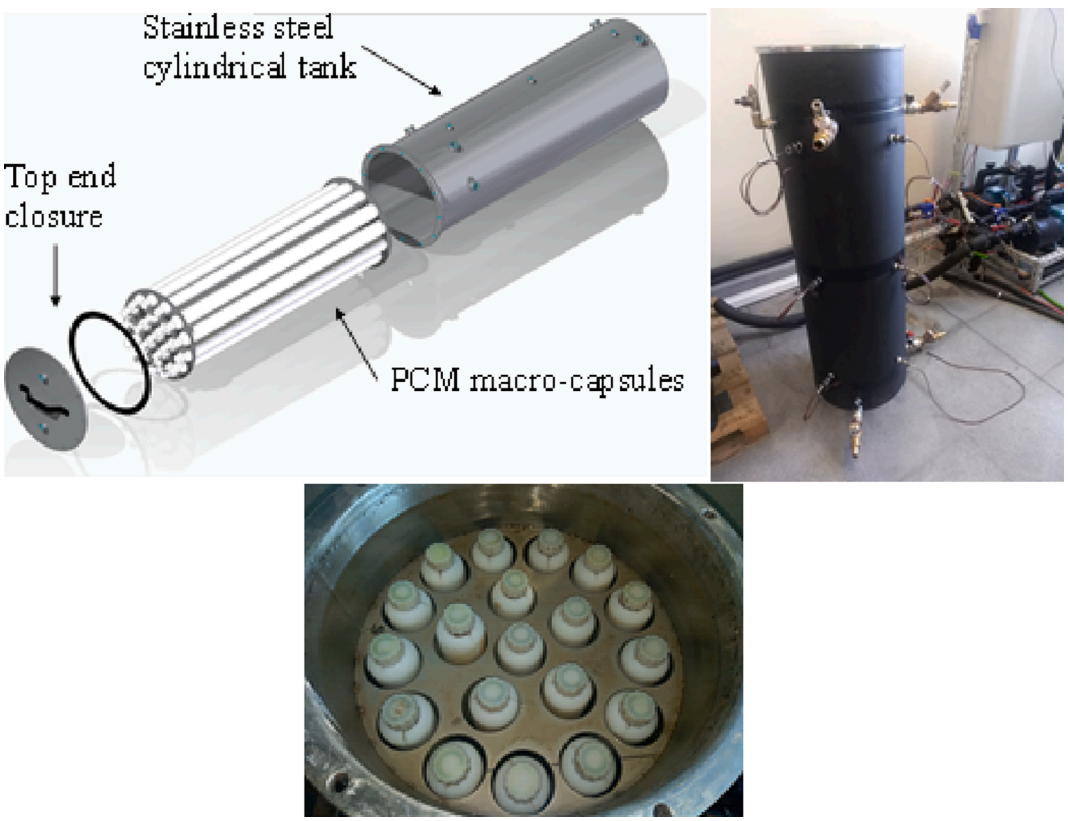

Fig. 7. Tri-dimensional view of the designed and realized lab-scale hybrid sensible/latent TES (top left); prototype instrumented and connected to the testing rig at CNR ITAE (top right); internal view of the hybrid TES with the macro-capsules inserted (bottom).

overall amount of PCM integrated inside the tank is 40 dm^3. The hybrid configuration allows exploiting the water both as storage medium and heat transfer fluid, thus maximising the heat transfer efficiency with the PCM macro-capsules.

The designed storage was manufactured and tested at the CNR ITAE lab. The detailed description of the TES as well as its thorough characterization and modelling are reported elsewhere [48]. An example of the dynamic evolution of the temperature measured inside the storage and the delivered thermal power is reported in Fig. 8. Three T-type thermocouples (Table 6 for details) were embedded inside the storage tank:

- top side, corresponding to the height of the exiting port of the water to the user;
- middle side, at half height of the tank;
- bottom side, corresponding to the height of the inlet port of the water from the user.

The thermocouples are in direct contact with the water, accordingly they are used to monitor the stratification inside the tank both during discharging and stand-by periods. Every discharging phase was protracted until the delivery temperature reached 40 °C. Afterwards, the flow was stopped and the temperatures inside the tank were monitored. As highlighted in Fig. 8, during the discharging phase no temperature gradient was revealed, meaning that a fully-mixed operation was achieved. Differently, during the stand-by periods the thermal energy released by the PCM heated up the surrounding water, due to the slow

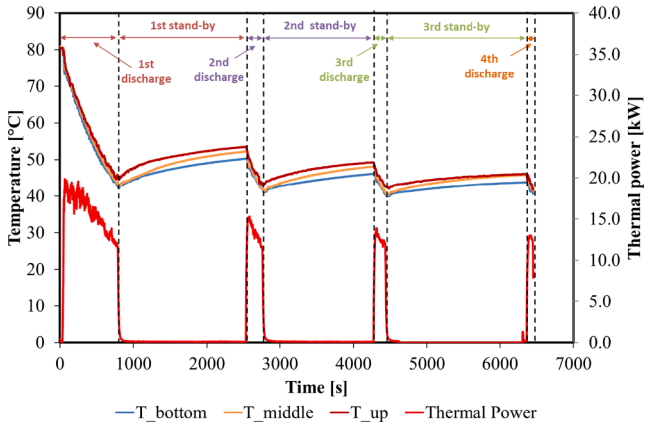

Fig. 8. Experimental evolution of the temperature inside the tank and thermal power delivered to the user by the TES, during consecutive discharging and stand-by periods, starting from 80 °C down to 40 °C.

phase change process. This allowed a subsequent discharging process even without a further charging of the storage. In this case, due to the difference in water density, a certain degree of stratification was achieved, with about 3 K from the bottom to the top of the storage. This reheating phase was exploited up to four times, thus achieving an overall storage density higher than the corresponding sensible storage configuration.

Energy charged/discharged was calculated as the integral of the instantaneous power for the whole duration of the charge/discharge process.

$$E = \int_0^{\tau_{fin}} \dot{m} c_p (T_{in} - T_{out}) \cdot d\tau \tag{3}$$

Energy density was calculated as the ratio of the discharged energy over total storage volume:

$$E_{volume} = \frac{E_{discharged}}{V_{storage}} \tag{4}$$

In order to analyse the heat transfer efficiency of the proposed solution, also the discharging power was evaluated for each stage, as represented in Fig. 8.

Furthermore, tests performed in a charging temperature range between 65 °C and 80 °C confirmed the possibility of achieving energy storage density from 29 kWh/m^3 to 52 kWh/m^3, which corresponds to an increasing from 20 % to 30 % compared to a pure sensible storage configuration. This demonstrates the possibility of reducing the volume occupied on-board to store and provide the thermal energy, thus either increasing the overall flexibility of the system or reducing the needed storage volume to cover the users demand.

3.4. The ORC sub-system

The market availability of 1–10 kW ORC units is very limited. Discarded the possibility of designing a prototype targeted on the characteristics of the ICE, due to the difficulty of finding some of the main components and to the excessively long realization time, the Kaymacor [49] small size ORC group was identified as compatible with the setup specifications in terms of technical characteristics and delivery time. Its main technical data are reported in Table 5.

In collaboration with Kaymacor, preliminary tests were carried out with the aim of better adapting the group to the project specifications. The variables taken into consideration were the operating fluid and the rotation speeds of pump and expander. The two speeds are fundamental control parameters because they respectively determine the flow rate of the operating fluid and its vaporization pressure. The possibility of adaptation of the group to the exploitation of thermal sources of different capacities and temperatures depends on these quantities [50,51].

As for the optimal choice of the operating fluid of the ORCs, the technical-scientific literature on the subject is very extensive. In this case, which does not refer to a basic thermodynamic study, as in most of the literature, but to the application of an existing group to a specific experimental facility, the choice is limited by the availability of the supplier, by the compatibility with the materials and with the volumetric capacity of the ORC components, in particular of both the pump and the expander. The fluid normally used in the Kaymacor group is R245fa, with the possibility of using R134a as an alternative, depending on the source temperature. Both fluids are positively considered in literature for low temperature applications, see for example [10,11,13], also thanks to their rather low critical temperature, equal to 101 °C for R134a and 154 °C for R245fa, as shown by the saturation diagrams of the two fluids in Fig. 9. Considering the maximum temperature of 100 °C of the available hot source, and the results of some preliminary tests, the R134a was finally chosen.

As for the rotation speeds of pump and expander, the limits set by the group's control system have been preliminarily identified. Speeds between 2780 and 3450 rpm have been then tested for the pump, with the best results at 3000 rpm. For the expander, the most appropriate speed immediately emerged to be the minimum one, equal to 1800 rpm. It has been kept constant, given the rather limited variation in the operating conditions of the system under which the control system activates the ORC group, so allowing also the production of electricity at constant frequency.

The unit has been specifically instrumented in order to detect the temperatures of superheated vapour at the expander inlet and of the subcooled liquid at the pump inlet, in addition to the vaporization and condensation pressures already measured in the standard configuration. Temperatures are measured with thermoresistances placed in contact with the external surface of the pipes in which the operating fluid flows, and thermally insulated from the external environment. More detail about the sensor used are reported in Table 6 in section 3. For this reason, in case of unsteady operating conditions, there will be a response delay in the temperature measurement, until the thermal equilibrium between fluid, pipe wall and sensor is reached. The flow rate of operating fluid is calculated as a function of the pump rotational speed, using its operating curves. They were previously measured, with the same

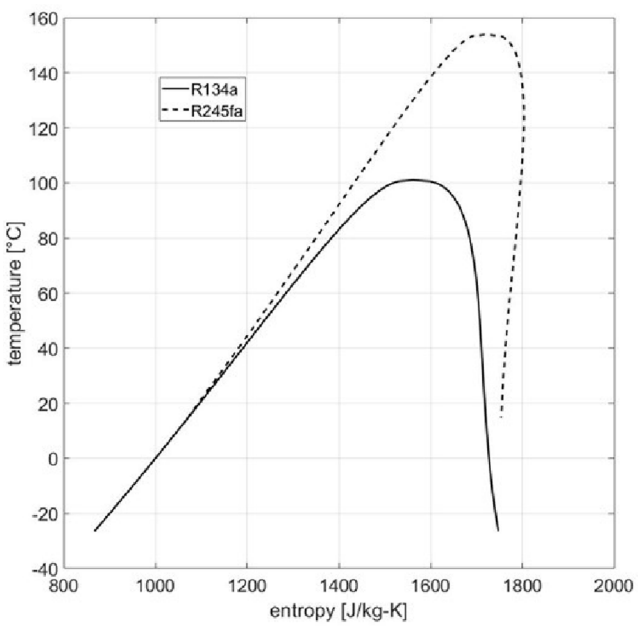

Fig. 9. Saturation curves of the considered ORC working fluids.

fluid, on the volumetric pump test bench at the EnesysLab of the University of Trieste [52]. The flow rates of the hot spring and cold well fluids are instead measured with the instrumentation of the test bench.

In the final installation at the CNR-STEMS, the direct use of hot water from the engine cooling circuit in the ORC evaporator was preferred to the use of an intermediate circuit with diathermic oil, normally provided for the Kaymacor groups.

The last one was discarded because it would have led, even without considering the cost and complication of the system, to a further lowering of the quality of the heat to be recovered. However, this required a verification of the thermal efficiency of the evaporator, based on the new operating specifications.

An example of measured cycle is shown in Fig. 10, together with the functional diagram of the unit. The horizontal red and cyan dotted lines correspond, as a thermal reference, to the inlet temperature of the engine hot water in the evaporator, t_{in} hot fluid, and of the cold water in the condenser, t_{in} cold fluid, respectively.

The obtained results are presented in Figs. 11 and 12. The first shows the temperatures (on the left) and the pressures (on the right) measured as a function of time. At the start of the unit, the temperature increase of the water of the ICE circuit is observed, followed in phase delay by that of the temperature of the superheated steam (or, more precisely, of the inlet temperature in the expander). This delay is due both to the dynamics of the evaporator and to the low frequency response of the temperature measuring arrangement. The only temperature that can be considered in phase is that of evaporation, because it is obtained with the equation of state of the fluid (using the CoolProp software) on the basis of the detected pressure value, which can be considered free from response delay.

The subsequent phase of operation at almost stationary conditions is obtained by also exploiting the energy stored in the TES. The useful observation window is between minute 2.5 and minute 4.5, a period in which the operating conditions are constant and all the temperature measurements can be considered reliable.

Fig. 12 shows that the net power produced in these conditions is about 1200 W, which is not to be neglected considering the maximum motor power of only 16 kW.

The efficiency of the ORC was also calculated, based on the following consideration: the installed group carries out a regenerative cycle, but the degree of regeneration (depending by the greater or lesser proximity of the temperature of the liquid leaving the regenerator to those of the expander outlet steam) cannot be evaluated based on the available data. Therefore, for each experimental point, the two possible extreme values of the yield have been calculated, that is for degrees of regeneration, R, equal to zero and one, respectively. In the case of R = 0, i.e. with the inlet enthalpy in the evaporator equal to the exit enthalpy from the pump, the efficiency is calculated with eq.1, where subscripts 5 and 2 have the meaning shown in Fig. 10, and $\dot{m}_{wf}$ is the R134a mass flow rate:

$$\eta_{ORC_{R=0}} = \frac{P_{el}}{(h_5 - h_2)\cdot\dot{m}_{wf}}\cdot 100 \tag{5}$$

In the case of R = 1, instead, the inlet enthalpy in the evaporator is supposed to be equal to the saturated liquid temperature of the working fluid at the evaporating pressure, and the efficiency is calculated with eq.2:

$$\eta_{ORC_{R=1}} = \frac{P_{el}}{(h_5 - h_3)\cdot\dot{m}_{wf}}\cdot 100 \tag{6}$$

The data thus obtained are shown in the right-hand diagram of Fig. 12: the real value will necessarily be between the two extremes. An average yield of 4–4.5 % is obtained, in good agreement with the expectations.

As explained in the next paragraphs, during the setting up of the control system, the thermal source temperatures at which it is convenient to start or stop the ORC was identified to maximise the efficiency of the system.

3.5. *Control and monitoring device*

An advanced control tool and the corresponding control algorithm have been developed in order to manage the energy flows as a function of the user demand and to register all the main control and output parameters of the prototype. These parameters are acquired and sent by a fast communication protocol to the prototype electronic control unit (ECU), where such information is managed to maximize the efficiency of the system according to both the heat availability and the source temperature. The ECU is also connected to the plant safety, supervision and alarm system.

More in details, the ECU function is to control:

- the SE operating state and speed, in accordance with a reference value based on the exhaust gas flow and temperature;
- the ORC operating state and pump rotational speed, in accordance with the inlet temperature of the hot fluid in the heater, which in turn depends on the exhaust gases residual heat as well as on the temperature of the ICE cooling water;
- the TES state, based on the prediction for the next hours of hot water consumption of the simulated ship and on the temperature of the ORC hot water circuit.

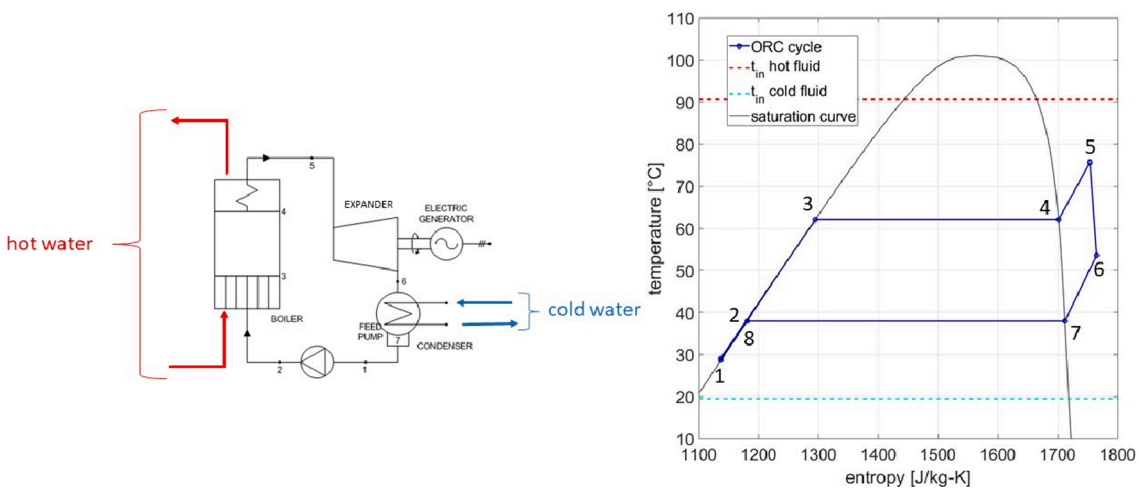

Fig. 10. Scheme of the ORC group and t-s diagram of the cycle with R134a.

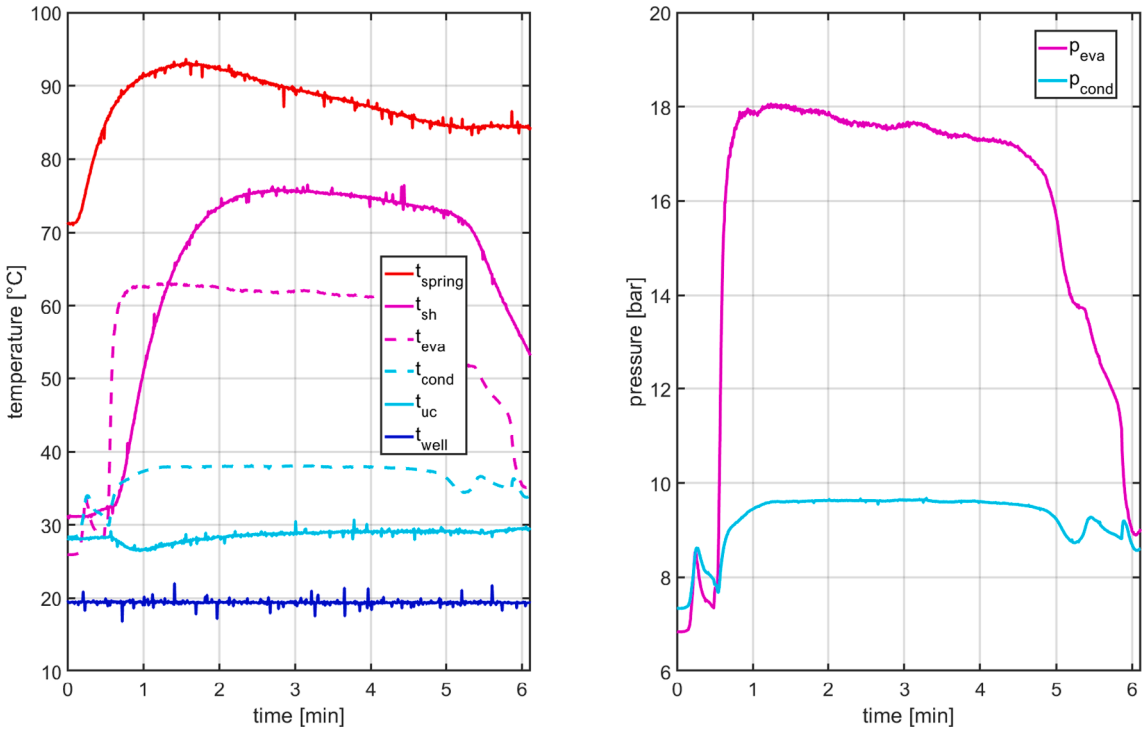

Fig. 11. Results of an initial ORC test (heat transfer fluid: ICE cooling water - operating fluid: R134a) left: temperatures of i) hot spring inlet, ii) superheating, evaporation, condensation and under-cooling of the organic fluid, iii) cold well inlet dx: evaporation and condensation pressures.

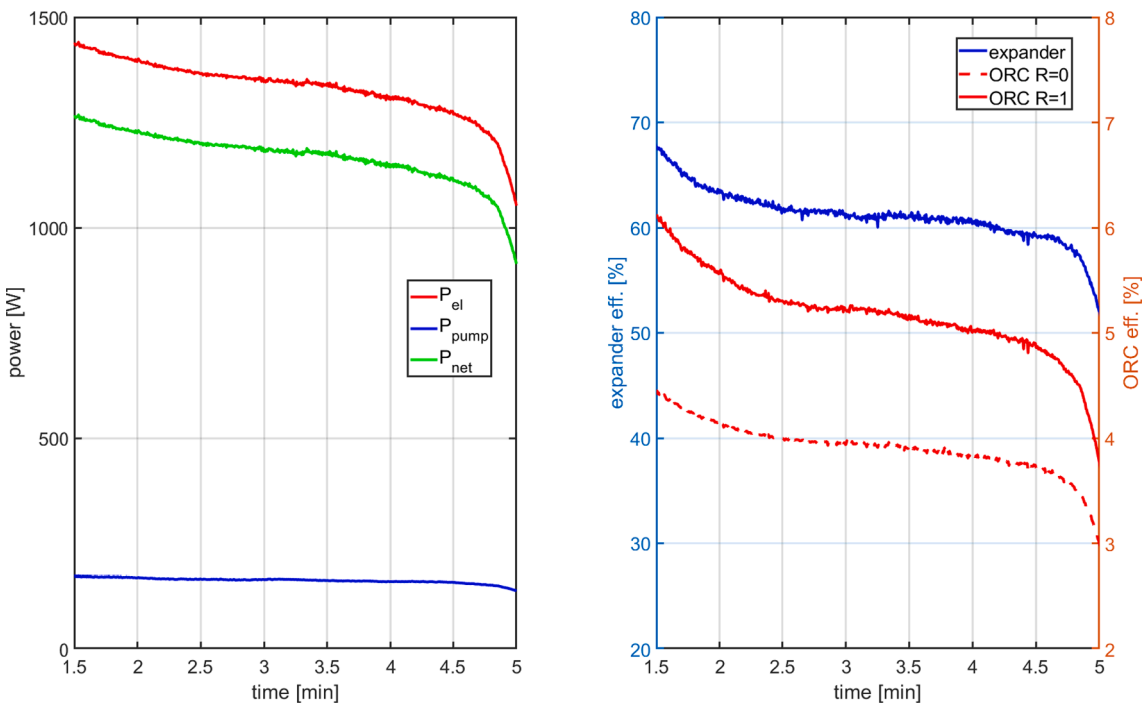

Fig. 12. Results of an initial ORC test (heat transfer fluid: ICE cooling water - operating fluid: R134a) left: gross electrical power, absorbed by the pump and net power dx: overall isentropic efficiency of the expander and the ORC (regeneration degree R = 0 and R = 1).

The block diagram of the control system is reported in Fig. 13.

4. Experimental procedure

The prototype was tested by simulating two different cruises. Fig. 14 shows the hypothesized ship engine power and thermal power consumption for hot water production [53] considered for the cruise 1 and cruise 2, respectively, in the top and bottom part of the figure. Three engine loads were considered to mimic the main cruise phases: sailing, maneuvering and stationing in the port. During the prototype laboratory testing, the various phases of the cruise have been carried out appropriately scaling both the time scale and the power request.

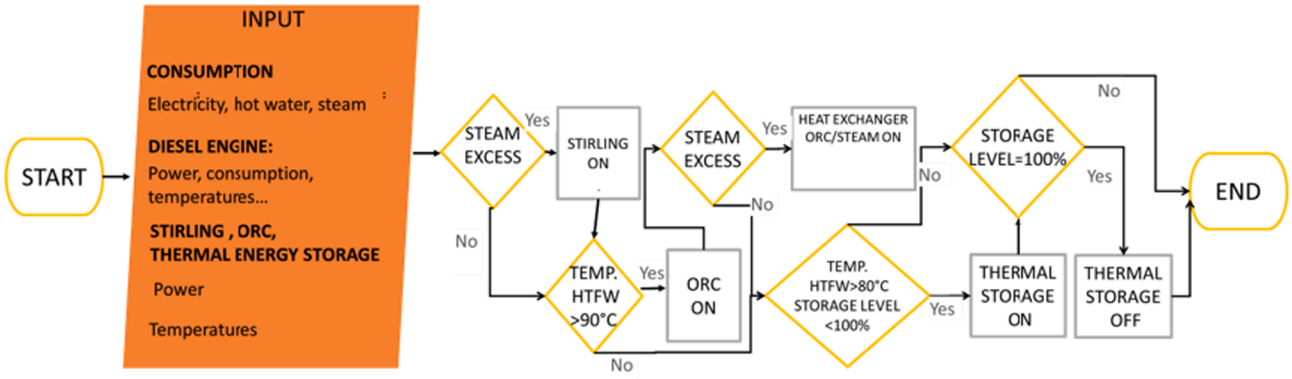

Fig. 13. Block diagram of the control system designed for the prototype.

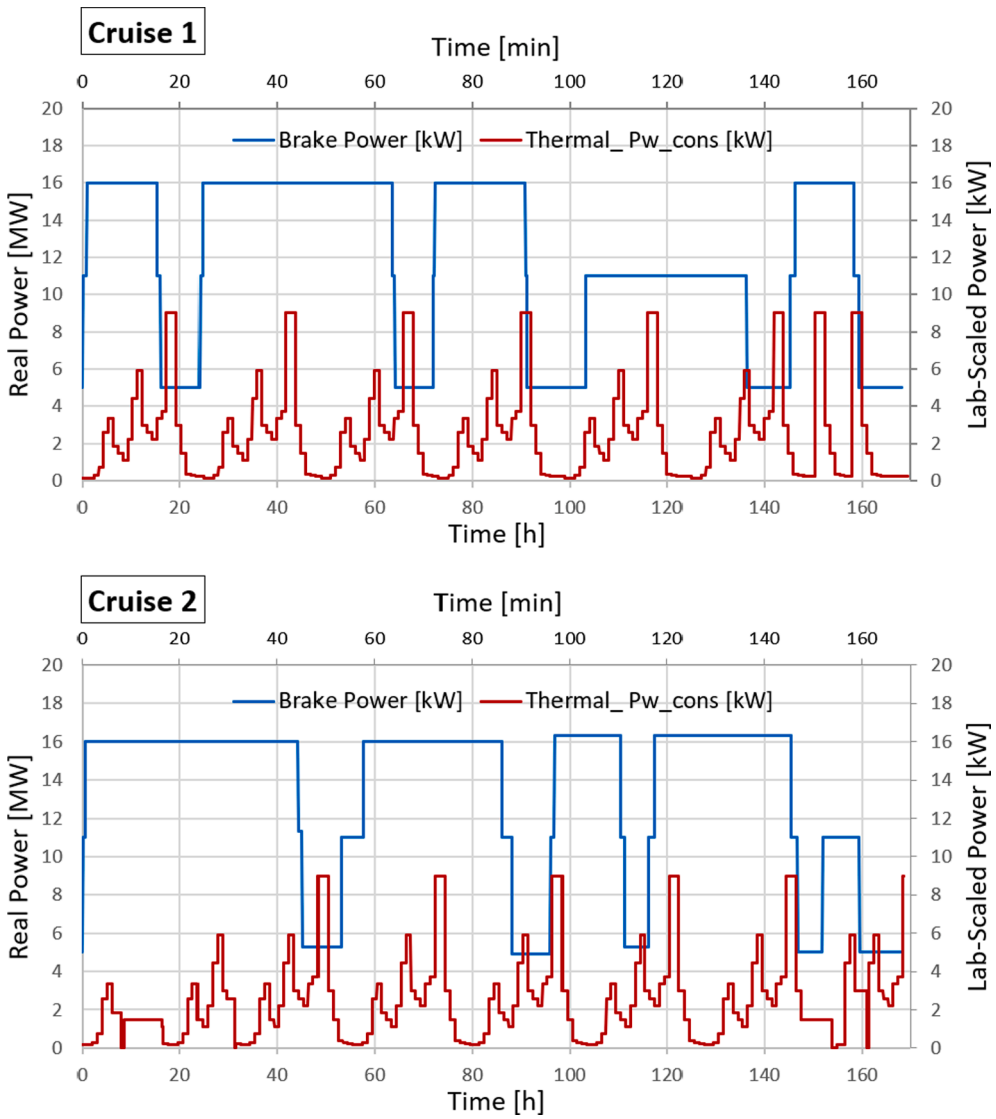

Fig. 14. Engine and thermal power profiles simulated in the lab-scaled experiment for cruise 1 and cruise 2.

The cruise time was scaled matching minutes to hours and thus each cruise lasted about 168 min instead of 168 h, i.e. one week. This allowed performing different tests in the same day, having also an important simplification of the experimental activity.

The engine loads were scaled by a factor of 1000, in order to simulate the aforementioned cruise phases as follows:

- in sailing conditions, the engine was kept at maximum load at 3400 rpm with about 16.4 kW of brake power;

- in maneuvering phases, the engine load, as well as in the real cruise, was fixed at about the 70 % of the maximum power, that is 11 kW;
- in port stationing, the engine load was kept close to idle, delivering about 5 kW of power. This corresponds to about the 30 % of the maximum power in both the real and scaled cruises.

The real cruise 1 lasted 168 h of which: 114.5 h in sailing condition with a maximum engine power for propulsion and electric generation of about 16 MW, 46 h in port stationing with a total power request for all the services of about 11 MW and 7.5 h consuming about 5 MW for maneuvering and additional services. Similar conditions were considered also for cruise 2, which differs from cruise 1 mainly for a slightly higher average engine power and a slightly lower thermal energy consumption, in order to evaluate the system also in different seasonal conditions.

The simulation of hot water consumption on the ship was carried out according to a typical hourly consumption profile. The thermal energy consumption was scaled in the laboratory tests by the same factor of 1000 chosen for the ICE power scaling. The hot water power consumption profile was considered the same for six of the seven days of both cruises while it was varied in the last day of cruise 1 introducing a more severe condition, characterized by three peaks of maximum thermal power request. On the other hand, in cruise 2 a lower thermal power was imposed in the first day of the cruise. As a whole, the total hot water energy consumption resulted to be higher in cruise 1 than in cruise 2 of about 10 %.

In the lab-scale experiment, in order to reproduce these consumption profiles, a properly sized heat exchanger endowed with an electric valve was arranged downstream the TES. Temperature upstream and downstream the heat exchanger, as well as the water flow, were monitored and controlled by means of an in-house control system, integrated in the monitoring device described in section 2.5, realized with a custom electronic board and a software developed in Labview. In particular, during the simulated cruise the hot water consumption profile was achieved keeping the hot water at the temperature of about 50 °C and controlling the water flow to match the power request. The frequency of the data acquisition and control was close to 50 Hz.

Table 6 summarizes the main features of the sensors used for the monitoring and control system. The error of the measurements was always lower than 3 % and no error bar has been reported in the figures in order to improve the readability.

5. Experimental results

Fig. 15 shows the brake power of the ICE and the total power actually recovered with the lab-scaled prototype during the whole cruise 1 simulated at the test bench. Particularly, the thermal power related to the hot water consumption, the SE electrical power and the net electrical power generated by the ORC, i.e. net of that absorbed by the pump, have been reported for the 168 min representing the seven days of the cruise with the scaling ratio described in the previous paragraph. It is evident that the main contribution to the energy recovery came from the thermal storage, due to the design choice of giving priority to the thermal storage over the other systems and also because it is not affected by the heat to work conversion efficiency.

The actual thermal power for hot water consumption obtained during the simulated cruise 1 is also reported in Fig. 16, together with the imposed request profile and the corresponding cumulative curves. Actual power is higher than the request one in most of the simulated cruise, confirming the capability of the system to provide all the thermal energy for passenger use, as it can be noted also looking at the actual total thermal energy that is always higher than the requested one.

The system has been able to provide enough thermal energy also in the most severe condition characterized by the two close maximum consumption peaks, simulated in the last 24 min (last day of the cruise). These results arose from the control strategy that keeps the temperature inside the storage close to the target temperature (60 °C) maximizing the exploitation of the latent heat storage capability.

Fig. 17 reports the temperatures measured inside the TES in the upper position (UP), in the lower position (DN), and in the half height position, along with the hot water temperature measured during the simulated cruise 1. The last one was always included in the interval 40–55 °C, typical operating range of hot water demand for sanitary use.

In order to control the temperature inside the TES, the ORC was activated when the storage temperature reach the maximum value (70 °C) and it was deactivated before the storage temperature was lower than the minimum value (55 °C). This control strategy is clearly shown in Fig. 18 that reports the time history of the ORC net power, together with the time evolution of the operating variables that have some influence on the ORC performance. The time considered interval is relative to a cruising phase of cruise 2, comprehensive of the starting and arriving manoeuvring conditions, with a total duration of 35 min of experimental time.

The following sequence of the ORC operating conditions is clearly

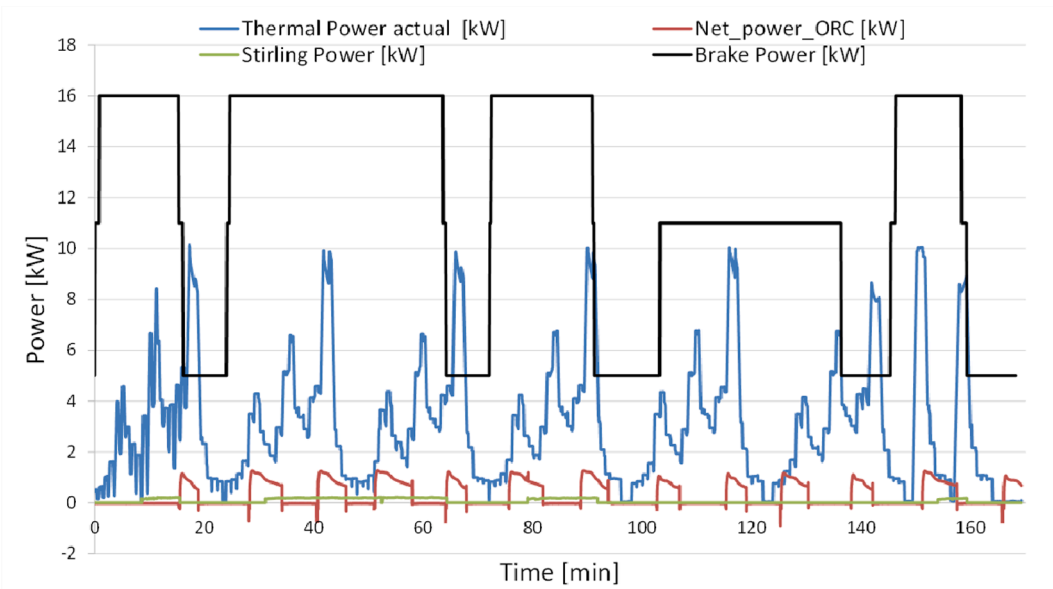

Fig. 15. Lab-scaled simulation of cruise 1: total power recovered with the WHR system and ICE brake power.

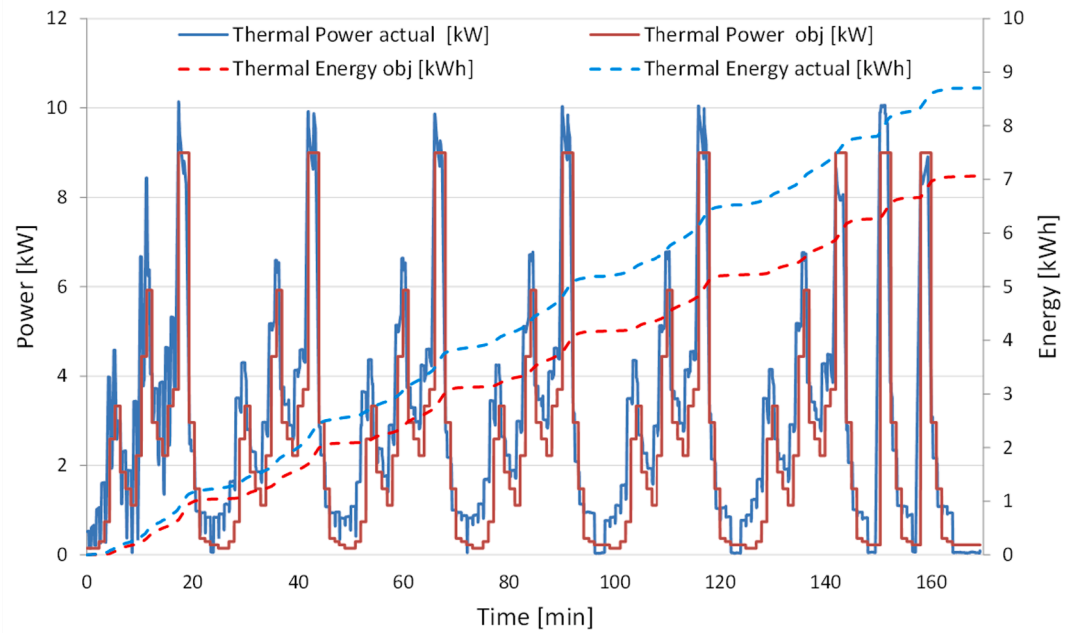

Fig. 16. Typical request profile and actual thermal power and total energy for hot water consumption obtained during the simulated cruise 1.

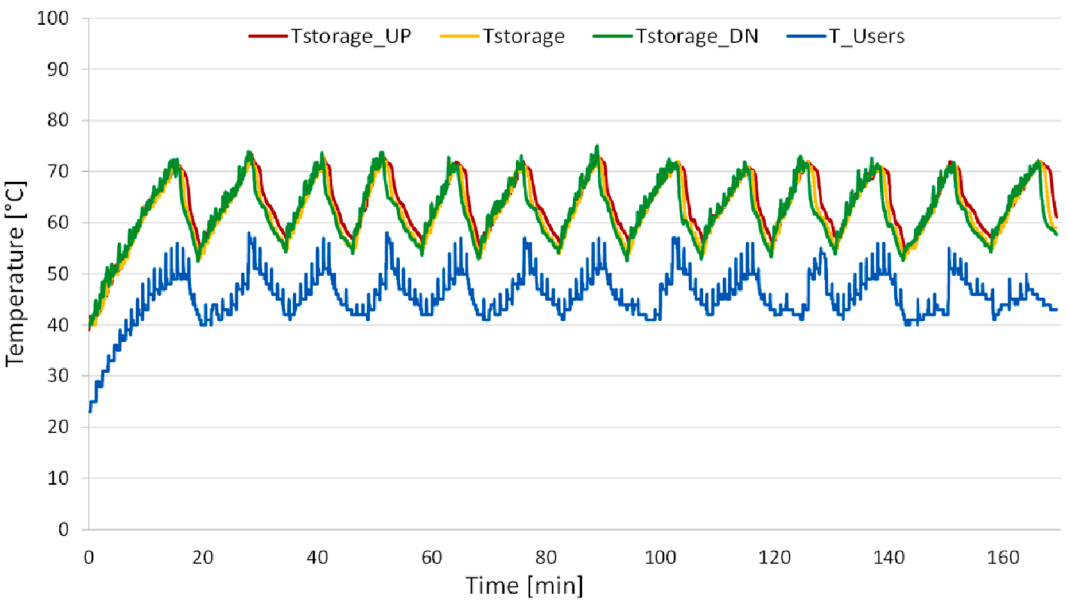

Fig. 17. Thermal storage inside temperatures, in the upper position (UP), in the lower area (DN), and in the center, and the hot water temperature measured during the simulated cruise 1.

shown:

- at time t = 119 min the engine load is set at its maximum value and the filling of the thermal storage is almost completed: the ORC is allowed to start;
- the switching of the pump of the ORC group causes a transient with negative net power until the pressure of the operating fluid reaches its equilibrium value. This occurs when the stationary heat balance of the evaporator allows achieving the super-heated vapour density that satisfies the volumetric flow rate required at the inlet of the expander. Then the group starts delivering power and quickly reaches a net value of about 1.25 kW, less than one minute after the pump switch on;
- then, the group net power gradually decreases. In fact, the temperature of the hot water entering the ORC, called t_{source} in the figure, decreases of about 1.2 °C/min, even if both the temperature of the gases leaving the SE (and entering the auxiliary heater dedicated to the ORC) and the ICE load are almost constant. This is due to the progressive emptying of the storage, which causes a progressive lowering of the temperature of the water entering the engine cylinder block;
- At time t = 125 min the temperature of the thermal storage drops to 55 °C, and another filling phase starts: by acting on the three-way valve, the flow of hot water in the ORC evaporator ends and the unit is automatically switched off.

As far as the effectiveness of the main heat exchangers of the ORC is

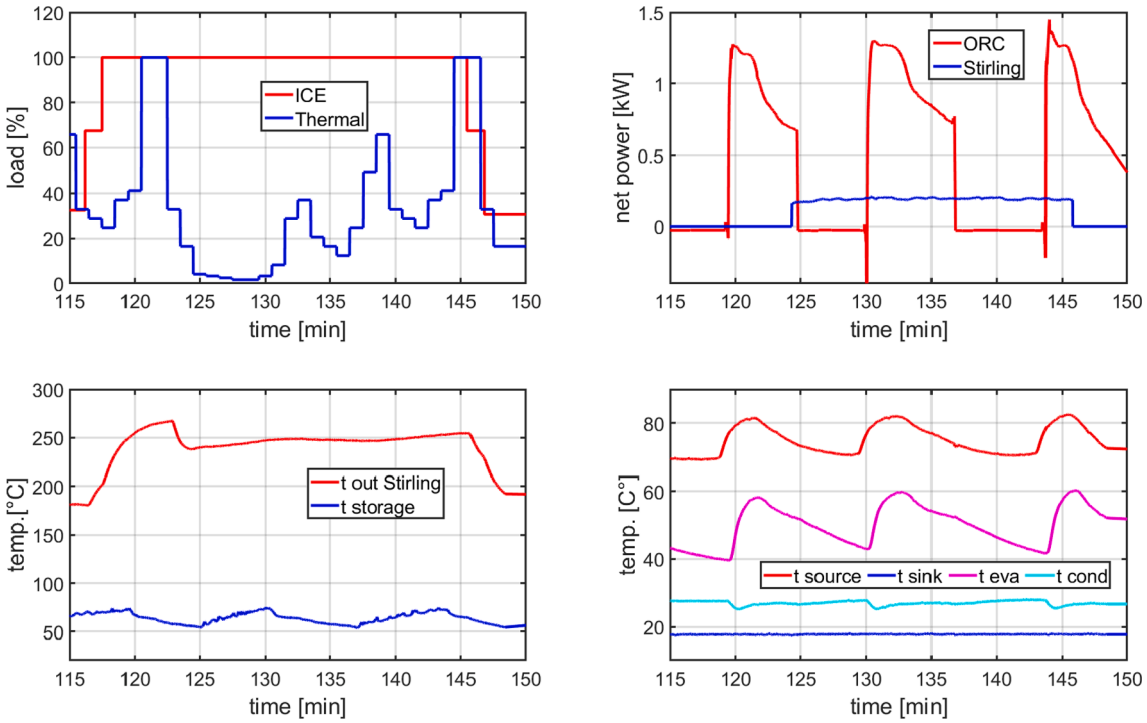

Fig. 18. Time history of the ORC net power and other boundary operating variables in a cruising phase, comprehensive of the starting and arriving maneuvering conditions, during the cruise 2.

concerned, Fig. 18 shows that:

- the temperature difference in the evaporator between the hot water entering the group and the superheated organic fluid remains almost constant, around 20 K: it is an acceptable result, considering that the evaporator is the original one, designed to operate with diathermic oil on the hot side, and not optimized for this specific application;
- the temperature difference in the condenser between the organic fluid and the cold water is constantly around 8–9 K, a value that can be considered acceptable.

Fig. 18 also depicts a working phase of the SE that started producing power with a delay of a few minutes after the ICE entered the navigation phase from a maneuvering condition, i.e. engine brake power passed from about 70 % to 100 %.

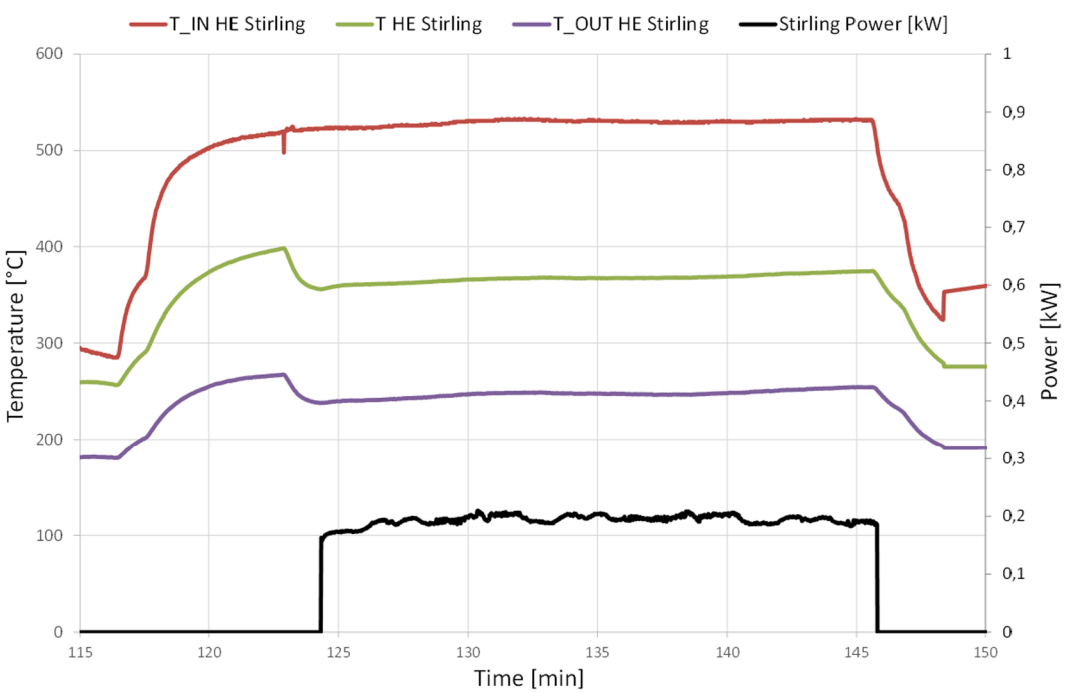

Fig. 19. SE heater internal temperature (T HE), at the inlet (T_IN HE) and at the outlet (T_OUT HE) during a transition phase between maneuvering and navigation phase of the simulated cruise 2.

To explain the cause of such a delay, Fig. 19 reports the temperatures at the inlet (T_IN HE), at the outlet (T_OUT HE) and inside (T HE) the Heat Exchanger (HE) of the SE during one of its complete switching on, power generation and shutdown processes, in the same time interval of Fig. 18. A transition between maneuvering and navigation phases of the simulated cruise is considered and it is evident that, as soon as the engine load increases, the T_IN HE curve shows a strong rise. Only when it overcomes 500 °C, the Stirling engine is started, activating the electric motor. This produces a decrease of both T_OUT HE and T HE caused by the strong heat subtraction due to the He heating phase. This phase lasts less than one minute and then the control switches the electric motor to the functioning as a generator, applying the electric load. Less than two minutes later the start, a quasi-steady state condition is reached, temperatures remain almost constant and the SE constantly produces about 200 W of power (which would correspond to about 400 kW in the real scaled system). Stirling engine is stopped and the electrical load is disconnected when the T_IN HE temperature became again lower than 500 °C, due to the decrease of the ICE load. All the three temperatures decrease and, particularly, T_OUT stabilizes at about 180 °C.

This control strategy was designed in order to both optimize the SE power production and to avoid an excessive decrease of exhaust gas temperature. It was preferred to avoid temperatures lower than 180 °C at the exhaust in order to prevent problem to the after-treatment system and to favor the operation of the steam production system, of the TES and of the ORC energy recovery, which is more efficient at a lower temperature.

This configuration of TES and ORC allows better result in term of total energy recovered by the WHR system. The drawing of hot water has priority over the operation of the ORC and the control unit during the test deactivates the latter when the temperature of the storage tank falls below 55 °C which corresponds to about 40 °C hot water leaving the secondary exchanger.

Similar results have been obtained for the both tested cruises, as reported in Fig. 20 in term of total energy recovered in comparison with the ICE energy consumption. The energy recovered as hot water covered the largest percentage of total energy with respect to fuel consumption. In particular, it was 7.7 % in the cruise 1 and 6.8 % in cruise 2 of the total energy consumed by fuel. In these simulated cruises with a duration of 168 min and small ICE (16 kW), the recovered energy resulted to be about 520 kWh and 500 kWh for cruise 1 and 2, respectively, which it could correspond for cruise 1 to 520 MWh and 500 MWh in cruise 2, considering the scaling factor of 1000 applied to the lab prototype. From the ORC and SE, the energy recoveries have been 0.8 % and 0.2 %, respectively, that corresponds to 53 kWh and 11.2 kWh for the cruise 1 and 75kWh and 16.3 kWh for the cruise 2.

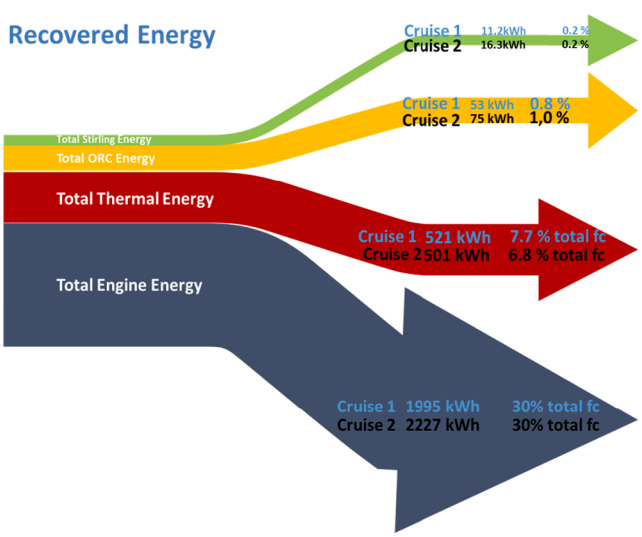

Fig. 20. Total energy recovered in comparison with the ICE energy consumption, for both cruises simulated at the test bench.

The described lab-scaled prototype of the energy recovery system was the most efficient of several configurations realized and tested at CNR-STEMS using the three WHR systems. In another configuration, the TES was acting also as energy storage for the ORC and all the waste heat of the exhaust gases was used only for the SE. This configuration allowed a slight improvement in the SE efficiency but a decrease in the efficiency of both TES and ORC. In particular, the ORC functioning was disadvantaged due to the low temperatures of the inlet water while the TES worked at too high temperatures, being not able to exploit the latent operation mode.

6. Conclusions

The approach proposed in this work is capable of estimating the benefits of a waste heat recovery strategy, size its components and operate them optimally. The challenge was to properly design and experimentally study an energy system able to increase the energy efficiency of ships by recovering waste heat from the ship's propulsion system. A lab-scaled prototype of the energy recovery system was realized. The propulsion system of the ship was simulated with a small diesel engine. Other core components are a thermal storage tank prototype with embedded Phase Change Materials (PCMs), a Organic Rankine cycle (ORC) system and a Stirling engine, both optimized for the specific application. The exhaust line of the diesel engine has been endowed with a proper design gas to gas heat exchanger in order to provide thermal energy to the Stirling engine. Moreover, the cooling system of the diesel engine has been modified to send the hot water from the engine alternately to the ORC or to the thermal storage in order to maximize the heat recovery. The hot water to ORC passes also through a gas to water heat exchanger at the exhaust of the Stirling engine simulating the steam economizer of the ship. This increases the water temperature to the ORC enhancing the efficiency of the system. Finally, a water to water heat exchanger and an electronic valve has been used at the thermal storage outlet in order to simulate the hot water request of the ship. An advanced control tool (ECU) was developed in order to manage and optimize the energy flows as a function of the user demand.

The experimental research facility described in this work, and the related control system, makes it possible to verify the effectiveness of the combined WHR technologies during a cruise. In particular, the possibility of simulating operational profiles typical of different categories of ships on a small scale, in terms of both size and time, greatly facilitates the experimental activity. In such a way it can be verified the possibility of satisfying the fulfilment of the IMO parameters EEDI and SEEMP.

The tests have shown that the proposed SE-ORC-TES integrated technology allows recovering all the thermal energy needed to cover the hot water request, during the typical trips of such a kind of ship, without the use of auxiliary boilers. Such recovered thermal energy, corresponding to about 8.7 kWh in the scaled experimental conditions, represented the 7.7 % of the total energy consumed by fuel. At the same time, the net electrical energy generated by ORC and SE resulted to be about 1 % of the total fuel energy consumption, respectively 0.8 % and 0.2 %. These are not very high percentage values, but corresponding on a real scale to significant powers and to reductions in costs and emissions of interest to ship owners. The production of electrical energy from thermal recovery could be slightly increased if it were possible to have devices optimized already in the design phase for the specific application, and not only in the phase of adjusting the regulation to the ship operating conditions.

Purpose of the experiments can also be in the future the validation of models for calculating the performance of components, such as Stirling engines or ORC groups and thermal storage systems, operating in compliance with the constraints relating to the specific application on board ships for a comparative study.

Declaration of Competing Interest

The authors declare that they have no known competing financial interests or personal relationships that could have appeared to influence the work reported in this paper.

Acknowledgments

The authors thank ing. Giuseppe Toniato of Kaymacor for the assistance provided in carrying out the adaptation and the preliminary tests of the ORC group.

The authors are sincerely grateful to Carlo Rossi and Bruno Sgammato for setting up the system and for their technical support in the experimental activities.

Funding

This work is part of a project funded by the Italian Ministry of Infrastructure and Transport (MIT) - Fincantieri.

References

[1] Nepomuceno de Oliveira MA, Szklo A, Castelo Branco DA. Implementation of Maritime Transport Mitigation Measures according to their marginal abatement costs and their mitigation potentials. Energy Policy 2022;160:112699.

[2] IMO, Energy Efficiency Measures, (2016). http://www.imo.org/en/OurWork/Environment/PollutionPrevention/AirPollution/Pages/Technical-and-Operational-Measures.aspx (accessed September 19, 2019).

[3] IMO, RESOLUTION MEPC.282(70), 2016. http://www.imo.org/en/KnowledgeCentre/IndexofIMOResolutions/Marine-Environment-Protection-Committee-(MEPC)/Documents/MEPC.282(70).pdf.

[4] Luz T, Moura P. 100% Renewable energy planning with complementarity and flexibility based on a multi-objective assessment. Appl Energy 2019;255:113819.

[5] Pandiyarajan V, Chinna Pandian M, Malan E, Velraj R, Seeniraj RV. Experimental investigation on heat recovery from diesel engine exhaust using finned shell and tube heat exchanger and thermal storage system. Appl Energy 2011;88:77–87. https://doi.org/10.1016/j.apenergy.2010.07.023.

[6] Bouman EA, Lindstad E, Rialland AI, Strømman AH. State-of-the-art technologies, measures, and potential for reducing GHG emissions from shipping – A review. Transp Res Part D Transp Environ 2017;52:408–21. https://doi.org/10.1016/J.TRD.2017.03.022.

[7] Singh DV, Pedersen E. A review of waste heat recovery technologies for maritime applications. Energy Convers Manag 2016;111:315–28. https://doi.org/10.1016/J.ENCONMAN.2015.12.073.

[8] Butrymowicz D, Gagan J, Łukaszuk M, Śmierciew K, Pawluczuk A, Zieliński T, et al. Experimental validation of new approach for waste heat recovery from combustion engine for cooling and heating demands from combustion engine for maritime applications. J Clean Prod 2021;290:125206.

[9] Shu G, Liang Y, Wei H, Tian H, Zhao J, Liu L. A review of waste heat recovery on two-stroke IC engine aboard ships. Renew Sustain Energy Rev 2013;19:385–401. https://doi.org/10.1016/J.RSER.2012.11.034.

[10] Mondejar ME, Andreasen JG, Pierobon L, Larsen U, Thern M, Haglind F. A review of the use of organic Rankine cycle power systems for maritime applications. Renew Sustain Energy Rev 2018;91:126–51. https://doi.org/10.1016/J.RSER.2018.03.074.

[11] Zhu S, Zhang K, Deng K. A review of waste heat recovery from the marine engine with highly efficient bottoming power cycles. Renew Sustain Energy Rev 2020;120:109611.

[12] van Biert L, Godjevac M, Visser K, Aravind PV. A review of fuel cell systems for maritime applications. J Power Sources 2016;327:345–64. https://doi.org/10.1016/J.JPOWSOUR.2016.07.007.

[13] Wang Z, Jiang Y, Han F, Yu S, Li W, Ji Y, et al. A thermodynamic configuration method of combined supercritical CO2 power system for marine engine waste heat recovery based on recuperative effects. Appl Therm Eng 2022;200:117645.

[14] Feng Y, Du Z, Shreka M, Zhu Y, Zhou S, Zhang W. Thermodynamic analysis and performance optimization of the supercritical carbon dioxide Brayton cycle combined with the Kalina cycle for waste heat recovery from a marine low-speed diesel engine. Energy Convers Manag 2020;206:112483.

[15] Pili R, Romagnoli A, Kamossa K, Schuster A, Spliethoff H, Wieland C. Organic Rankine Cycles (ORC) for mobile applications – Economic feasibility in different transportation sectors. Appl Energy 2017;204:1188–97. https://doi.org/10.1016/J.APENERGY.2017.04.056.

[16] Mondejar ME, Ahlgren F, Thern M, Genrup M. Quasi-steady state simulation of an organic Rankine cycle for waste heat recovery in a passenger vessel. Appl Energy 2017;185:1324–35. https://doi.org/10.1016/J.APENERGY.2016.03.024.

[17] M. Casisi, P. Pinamonti, M. Reini, Increasing the Energy Efficiency of an Internal Combustion Engine for Ship Propulsion with Bottom ORCs, Appl. Sci. 2020, Vol. 10, Page 6919. 10 (2020) 6919. https://doi.org/10.3390/APP10196919.

[18] J. Song, Y. Song, C. wei Gu, Thermodynamic analysis and performance optimization of an Organic Rankine Cycle (ORC) waste heat recovery system for marine diesel engines, Energy. 82 (2015) 976–985. https://doi.org/10.1016/J.ENERGY.2015.01.108.

[19] Mat Nawi Z, Kamarudin SK, Sheikh Abdullah SR, Lam SS. The potential of exhaust waste heat recovery (WHR) from marine diesel engines via organic rankine cycle. Energy 2019;166:17–31. https://doi.org/10.1016/J.ENERGY.2018.10.064.

[20] Yang MH, Yeh RH. Thermodynamic and economic performances optimization of an organic Rankine cycle system utilizing exhaust gas of a large marine diesel engine. Appl Energy 2015;149:1–12. https://doi.org/10.1016/J.APENERGY.2015.03.083.

[21] Rech S, Zandarin S, Lazzaretto A, Frangopoulos CA. Design and off-design models of single and two-stage ORC systems on board a LNG carrier for the search of the optimal performance and control strategy. Appl Energy 2017;204:221–41. https://doi.org/10.1016/J.APENERGY.2017.06.103.

[22] Riffat S, Aydin D, Powell R, Yuan Y. Overview of working fluids and sustainable heating, cooling and power generation technologies. Int J Low-Carbon Technol 2017;12:369–82. https://doi.org/10.1093/IJLCT/CTX008.

[23] Scaccabarozzi R, Tavano M, Invernizzi CM, Martelli E. Comparison of working fluids and cycle optimization for heat recovery ORCs from large internal combustion engines. Energy 2018;158:396–416. https://doi.org/10.1016/J.ENERGY.2018.06.017.

[24] Yang J, Ye Z, Yu B, Ouyang H, Chen J. Simultaneous experimental comparison of low-GWP refrigerants as drop-in replacements to R245fa for Organic Rankine cycle application: R1234ze(Z), R1233zd(E), and R1336mzz(E). Energy 2019;173:721–31. https://doi.org/10.1016/J.ENERGY.2019.02.054.

[25] Invernizzi CM. Stirling engines using working fluids with strong real gas effects. Appl Therm Eng 2010;30(13):1703–10.

[26] Thombare DG, Verma SK. Technological development in the Stirling cycle engines. Renew Sustain Energy Rev 2008;12(1):1–38.

[27] Abuelyamen A, Ben-Mansour R. Energy efficiency comparison of Stirling engine types (α, β, and γ) using detailed CFD modeling. Int J Therm Sci 2018;132:411–23. https://doi.org/10.1016/J.IJTHERMALSCI.2018.06.026.

[28] Tlili I, Vakkar A. Thermodynamic analysis and optimization of solar thermal engine: Performance enhancement. Phys A Stat Mech Its Appl 2020;540:123012.

[29] Açıkkalp E, Kandemir SY, Ahmadi MH. Solar driven Stirling engine - chemical heat pump - absorption refrigerator hybrid system as environmental friendly energy system. J Environ Manage 2019;232:455–61. https://doi.org/10.1016/j.jenvman.2018.11.055.

[30] Naseri A, Bidi M, Ahmadi MH, Saidur R. Exergy analysis of a hydrogen and water production process by a solar-driven transcritical CO2 power cycle with Stirling engine. J Clean Prod 2017;158:165–81. https://doi.org/10.1016/j.jclepro.2017.05.005.

[31] Catapano F, Perozziello C, Vaglieco BM. Heat transfer of a Stirling engine for waste heat recovery application from internal combustion engines. Appl Therm Eng 2021;198:117492.

[32] Pereira J, Cunha D, Eames P. Thermal energy storage for low and medium temperature applications using phase change materials â€“ A review. Appl Energy 2016;177:227–38. https://doi.org/10.1016/j.apenergy.2016.05.097.

[33] Ouyang T, Wang Z, Zhao Z, Lu J, Zhang M. An advanced marine engine waste heat utilization scheme: Electricity-cooling cogeneration system integrated with heat storage device. Energy Convers Manag 2021;235:113955.

[34] Li H, Wang W, Yan J, Dahlquist E. Economic assessment of the mobilized thermal energy storage (M-TES) system for distributed heat supply. Appl Energy 2013;104:178–86. https://doi.org/10.1016/J.APENERGY.2012.11.010.

[35] Baldi F, Gabrielii C, Melino F, Bianchi M. A Preliminary Study on the Application of Thermal Storage to Merchant Ships. Energy Procedia 2015;75:2169–74. https://doi.org/10.1016/J.EGYPRO.2015.07.364.

[36] Fang S, Fang Y, Wang H, Liu Lu. Optimal Heterogeneous Energy Storage Management for Multienergy Cruise Ships. IEEE Syst J 2020;14(4):4754–64. https://doi.org/10.1109/JSYST.2020.2966711.

[37] Palomba V, Brancato V, Frazzica A. Thermal performance of a latent thermal energy storage for exploitation of renewables and waste heat: An experimental investigation based on an asymmetric plate heat exchanger. Energy Convers Manag 2019;200:112121. https://doi.org/10.1016/j.enconman.2019.112121.

[38] Eppinger B, Zigan L, Karl J, Will S. Pumped thermal energy storage with heat pump-ORC-systems: Comparison of latent and sensible thermal storages for various fluids. Appl Energy 2020;280:115940.

[39] Di Battista D, Fatigati F, Carapellucci R, Cipollone R. Inverted Brayton Cycle for waste heat recovery in reciprocating internal combustion engines. Appl Energy 2019;253:113565.

[40] Qu J, Feng Y, Zhu Y, Zhou S, Zhang W. Design and thermodynamic analysis of a combined system including steam Rankine cycle, organic Rankine cycle, and power turbine for marine low-speed diesel engine waste heat recovery. Energy Convers Manag 2021;245:114580.

[41] Barone G, Buonomano A, Forzano C, Palombo A, Vicidomini M. Sustainable energy design of cruise ships through dynamic simulations: Multi-objective optimization for waste heat recovery. Energy Convers Manag 2020;221:113166.

[42] Baldi F, Johnson H, Gabrielii C, Andersson K. Energy and exergy analysis of ship energy systems–the case study of a chemical tanker. Int J Thermodyn 2015;18(2):82. https://doi.org/10.5541/ijot.5000070299.

[43] Magno A, Mancaruso E, Vaglieco BM. Effects of both blended and pure biodiesel on waste heat recovery potentiality and exhaust emissions of a small CI (compression ignition) engine. Energy 2015;86:661–71.

[44] Urieli I, Berchowitz DM. Stirling Cycle Engine Analysis. Adam Hilger; 1984.

[45] Alfarawi S, AL-Dadah R, Mahmoud S. Enhanced thermodynamic modelling of a gamma-type Stirling engine. Appl Therm Eng 2016;106:1380–90.
[46] Li R, Grosu L, Li W. New polytropic model to predict the performance of beta and gamma type Stirling engine. Energy 2017;128:62–76.
[47] Sowale A, Kolios AJ, Fidalgo B, Somorin T, Parker A, Williams L, et al. Tyrrel Thermodynamic analysis of a gamma type Stirling engine in an energy rercovery system. Energy Convers Manage 2018;165:528.
[48] A. Frazzica, V. Palomba, V. Brancato, A. Freni, M. Manzan. Numerical simulation and experimental analysis of a latent thermal energy storage for naval applications, Eurotherm Seminar #112, Lleida 15-17 May 2019.
[49] https://www.kaymacor.com/it, September 2021 [Online].
[50] Carraro G, Bori V, Lazzaretto A, Toniato G, Danieli P. Experimental investigation of an innovative biomass-fired micro-ORC system for cogeneration applications. Renewable Energy 2020;161:1226–43.
[51] Carraro G, Rech S, Lazzaretto A, Toniato G, Danieli P. Dynamic simulation and experiments of a low-cost small ORC unit for market applications. Energy Convers Manage 2019;197:111863. https://doi.org/10.1016/j.enconman.2019.111863.
[52] S. Clemente, D. Micheli, R. Radu. G. Toniato, Experimental tests on a gear pump for organic Rankine cycle applications, in Microgen III: Proceedings of the 3rd edition of the International Conference on Microgeneration, Napoli, 2013.
[53] Manzan M, Pezzi A, Zandegiacomo de Zorzi E, Freni A, Frazzica A, Vaglieco BM, et al. Potential of thermal storage for hot potable water distribution in cruise ships. Energy Procedia 2018;148:1105–12. ISSN: 1876-6102.